Electronic Supplementary Information

Layered Manganese Oxides for Water-Oxidation: Alkaline Earth Cations Influence Catalytic Activity in a Photosystem II-like Fashion

Mathias Wiechen,[a] Ivelina Zaharieva,[b] Holger Dau*[b] and Philipp Kurz*[a]

[a] *Institut für Anorganische Chemie, Christian-Albrechts-Universität zu Kiel, 24118 Kiel, Germany.*
Fax: +49 431 880 1520; Tel: +49 431 880 5803,
E-mail: phkurz@ac.uni-kiel.de

[b] *Fachbereich Physik, Freie Universität Berlin, Arnimallee 14, 14195 Berlin, Germany.*
Fax: +49 30 838 56299; Tel: +49 30 838 53581,
E-mail: holger.dau@fu-berlin.de

Synthesis of M-birnessites

For the synthesis of M-birnessites **1-7**, three solutions were prepared, according to a route published by Luo *et al.*.[1]

1) KOH or NaOH were dissolved in 30 mL H_2O (see Table S1).
2) 3.92 g (16 mmol) $Mn(AcO)_2 \cdot 4\ H_2O$ and alkaline earth salts (see Table S1) were dissolved in 30 mL H_2O.
3) 984 mg (6 mmol) $KMnO_4$ were dissolved in 100 mL H_2O.

Solution 2) was now added dropwise in 10 min under vigorous stirring to 1), resulting in an off-white to light brown suspension. Subsequently, 3) was added dropwise to the suspension of 1) and 2) in 30 min under vigorous stirring. The obtained dark brown suspension was stirred for 3 d at 40 °C. Then, the precipitate was filtered off and washed with 1 L H_2O, before it was dried at 65 °C over a period of 16 h. For details see Table S1.

Table S1. Details of solutions 1) and 2) for the synthesis of M-birnessites 1-7.

	Base for solution 1)	Alkaline earth salts for solution 2)
$K_{0.31}$-birnessite (**1**)	14.0 g (250 mmol) KOH	56 mg (0.3 mmol) $Ca(AcO)_2 \cdot H_2O$
$Ca_{0.14}$-birnessite (**2**)	10.0 g (250 mol) NaOH	564 mg (3.2 mmol) $Ca(AcO)_2 \cdot H_2O$
$Ca_{0.27}$-birnessite (**3**)	14.0 g (250 mmol) KOH	1.13 g (6.4 mmol) $Ca(AcO)_2 \cdot H_2O$
$Sr_{0.18}$-birnessite (**4**)	14.0 g (250 mmol) KOH	677 mg (3.2 mmol) $Sr(NO_3)_2$
$Sr_{0.27}$-birnessite (**5**)	14.0 g (250 mmol) KOH	1.35 g (6.4 mmol) $Sr(NO_3)_2$
$Mg_{0.13}$-birnessite (**6**)	10.0 g (250 mol) NaOH	686 mg (3.2 mmol) $Mg(AcO)_2 \cdot 4\ H_2O$
$Mg_{0.28}$-birnessite (**7**)	14.0 g (250 mmol) KOH	1.37 g (6.4 mmol) $Mg(AcO)_2 \cdot 4\ H_2O$

Physical measurements

TG

TG analyses were done using a Netzsch STA 429DT - TG device. The samples were heated to 1000°C at a rate of 4 K min^{-1} under a flow of air (75 mL min^{-1}) in Al_2O_3 crucibles. The TG data were corrected for buoyancy and current effects.

AAS

Manganese atomic absorption spectroscopy (AAS) was performed on an AAnalyst spectrometer system by PerkinElmer.

Prior to analysis, about 10mg of the oxide samples were carefully weighed, suspended in 3 mL of a mixture of concentrated HNO_3 and 30 % H_2O_2 (2:1) and left at room temperature for 12 h. The obtained clear solutions were then diluted to 50 mL. 1 mL of the diluted solution was again diluted to 50 mL and then analysed by AAS.

Table S2. Manganese content in the synthesised M-birnessites

	µmol(Mn)/mg(Sample)
$K_{0.31}$-birnessite (**1**)	10.3
$Ca_{0.14}$-birnessite (**2**)	7.4
$Ca_{0.27}$-birnessite (**3**)	8.0
$Sr_{0.18}$-birnessite (**4**)	9.5
$Sr_{0.27}$-birnessite (**5**)	10.7
$Mg_{0.13}$-birnessite (**6**)	7.7
$Mg_{0.28}$-birnessite (**7**)	11.4

Energy dispersive X-ray spectroscopy

Energy dispersive X-ray fluorescence (EDX)/scanning electron microscopy (SEM) were carried out with a Philips ESEM XL30 equipped with an EDAX detector. The compositions are the result of averaging multiple independent measurements from a given sample.

BET analysis

N_2 physisorption isotherms were measured with a BelsorpMAX (**1**, **2**, **6**, **7**) and a BelsorpMINI (**3**, **4**, **5**) instrument respectively, and analysed according to BET theory in order to investigate surface areas.

X-ray powder diffractometry

The X-ray powder patterns were measured in reflection geometry using a PANalytical X'Pert PRO instrument.

IR

ATR-infrared spectra of the solid oxide powders were obtained using a Bruker Alpha P spectrometer.

X-ray absorption spectroscopy

Collection of X-ray absorption data. X-ray absorption data were collected at the KMC1 beamline at the BESSY synchrotron (Helmholtz-Zentrum Berlin, Germany) at 20 K in a liquid-helium cryostat (Oxford) with 150 mbar He gas in the sample chamber used for heat exchange. Measurements at the Mn *K*-edge were performed in absorption mode and detected by a home-made ionisation chamber. Incident energy in the range 6400-7570 eV was selected by Si111 double crystal monochromator. The Mn oxide powders were mixed with boron nitride in a 1:10 ratio to get an optical thickness of the sample of around unity (10-fold drop of the X-ray intensity after the edge). As an internal energy standard the simultaneously measured in absorption mode narrow pre-edge of $KMnO_4$ powder was used (energy position of the pre-edge was set to 6543.3 eV).

Initial data processing. After correction of the energy scale, equivalent scans were averaged. The slope of the pre-edge scattering background was removed by subtraction of a line with a slope determined from the absorption decrease before the Mn edge. In the post-edge range the hypothetical EXAFS-free absorption was determined by a third-order polynomial fit. For normalization the spectra were divided by this polynomial.
XANES: The given *K*-edge energies were determined by the integral method outlined in ref.[2]
EXAFS: For extraction of EXAFS spectra, the background was removed by subtraction of a cubic spline. The energy axis (*E*-space, in eV) of the EXAFS spectra was converted to an equidistant wavenumber axis (*k*-space, in $Å^{-1}$) according to

$$k = \sqrt{\frac{2m(E - E_0)}{\hbar^2}}$$

with *m* mass of the electron, the reduced Planck constant indicated by a crossed *h*, and E_0 = 6547 eV. The transition to an equidistant *k*-axis involved a reduction of the number of data points to 180.
The resulting spectra ($\chi(k)$ versus *k*) were weighted by k^3 to compensate for the drop in EXAFS oscillations with energy. All *R*-space spectra shown in the figures were obtained by Fourier transformation of k^3-weighted data in the range 2.7 – 16.9 $Å^{-1}$ (corresponding to energy range 6570-7570 eV). For these transformations a fractional cosine window was used (at the low-*k* side the window extends over 10% and at the high-*k* side over 30% of the *k* range).

EXAFS simulations. EXAFS simulations by least squares curve fitting of k^3-weighted oscillations in the *k*-space were performed using the in-house software SimX3 according to the equation:[3, 4]

$$\chi(k) = S_0^2 \cdot \sum_{i}^{n_{shell}} \Re \cdot \frac{N_i Feff_i}{kR_i^2} \cdot \exp(-2R_i/\lambda_i) \cdot \sin(2k \cdot R_i + \phi eff_i + \phi_i) \cdot \exp(-2\sigma_i^2 \cdot k^2)$$

where the sum goes over the atomic shells (groups of elements with the same atomic number and similar distances from the X-ray absorbing atom), S_0^2 is the amplitude reduction factor, $\Re$ is the total central atom loss factor, *Feff* is the effective curved-wave backscattering amplitude, N_i is the number of neighbours in the i_{th} atomic shell, R_i is the distance between the X-ray absorbing Mn atom and the atoms in the i_{th} atomic shell (backscatterer), λ is the mean free path in Å, ϕeff is the phase shift for each shell, is the total central atom phase shift, and σ_i is the Debye-Waller parameter of the i_{th} atomic shell (variation of distances around the average R_i). The functions $\Re$, *Feff*, λ, ϕeff and ϕ were calculated by Feff-8.4[4, 5] (self-consistent field option activated). The amplitude reduction factor S_0^2 was 0.8.

The coordination number, *N*, the distance, *R*, and the Debye-Waller parameter, $2\sigma^2$, were determined for each backscatterer shell by a least-squares fit of the calculated EXAFS. In the fit, the sum of squared differences between k^3 weighted experimental and calculated data in *k* space, was minimized in the energy range between 6560 and 7570 eV. This minimized value of the sum is denoted in the following as ε_m. The minimum was found by Levenberg-Marquardt algorithm with numerically calculated derivatives.[6]

Error range estimation. To estimate the error ranges for the obtained parameters, we used a procedure as outlined below. After parameters had been optimized, the experimental and the model curves were Fourier-isolated according to the following protocol: (1) Fourier transform from *k*-space to *R*-space for data corresponding to the *k*-range of 1.6 Å^{-1} to 16.9 Å^{-1}, without using a window function; (2) back transformation from *R*-space to *k*-space for data corresponding to the *R* range from 0.0 Å to 5.0 Å. The sum of squared differences between the Fourier-filtered experimental and calculated data in *k* space was calculated and denoted as ε_m*.
The degree of freedom of EXAFS simulations, ν, is defined as the difference between the number of independent experimental data points and the number of simulation parameters. The number of independent data points is estimated according to: $N_{ind} \approx 2\,\Delta k\,\Delta R / \pi$[7], where the simulation range corresponds to Δk = 15.3 Å^{-1} and ΔR-value was 2.5 Å (the simulated peaks in the Fourier transformed spectra were the first two peaks between 1 and 3 Å, and the peak between 4.5 and 5 Å on the scale of the reduced distances, see Fig. S1 and S2).
The recalculated error sum, ε_m*, and the degrees of freedom, ν, were used to normalize the original error sum, ε_m, according to the equation:

$$\varepsilon_m^{norm} = \nu \cdot \frac{\varepsilon_m}{\varepsilon_m^*}$$

For each fit parameter the respective 1σ-error range (68% confidence interval) corresponded to an increase in the normalized error sum by one[8]. The 1-σ-error range was obtained from the square root of the corresponding diagonal element of the covariance matrix of the system.

Quality of the fit. The R_F-factor given in Tables S3 and S4 is used to estimate the quality of the fit[9]. It was calculated according to

$$R_f = \frac{\sum_i \left|\chi_i^* - y_i^*\right|}{\sum_i \left|y_i^*\right|} \cdot 100$$

where χ_i^* and y_i^* denote k^3 weighted calculated and experimental data after Fourier isolation, using a cosine window function (10% at low-*k* and 30% at high-*k* side). The *R*-range was between 0 Å and 5 Å. In contrast to the unfiltered R^{error}-value, R_F does neither depend on the fit quality outside of the considered *R*-range nor on the number of *k*-space data points chosen during the transition from energy to wavevector scale (note that '*R'* may denote either a distance or a measure of the error in a least-squares fit, depending on the context). Fourier-filtering was employed only for calculation of the R_F-value (after curve-fitting); for curve-fitting itself exclusively unfiltered *k*-spectra had been used.

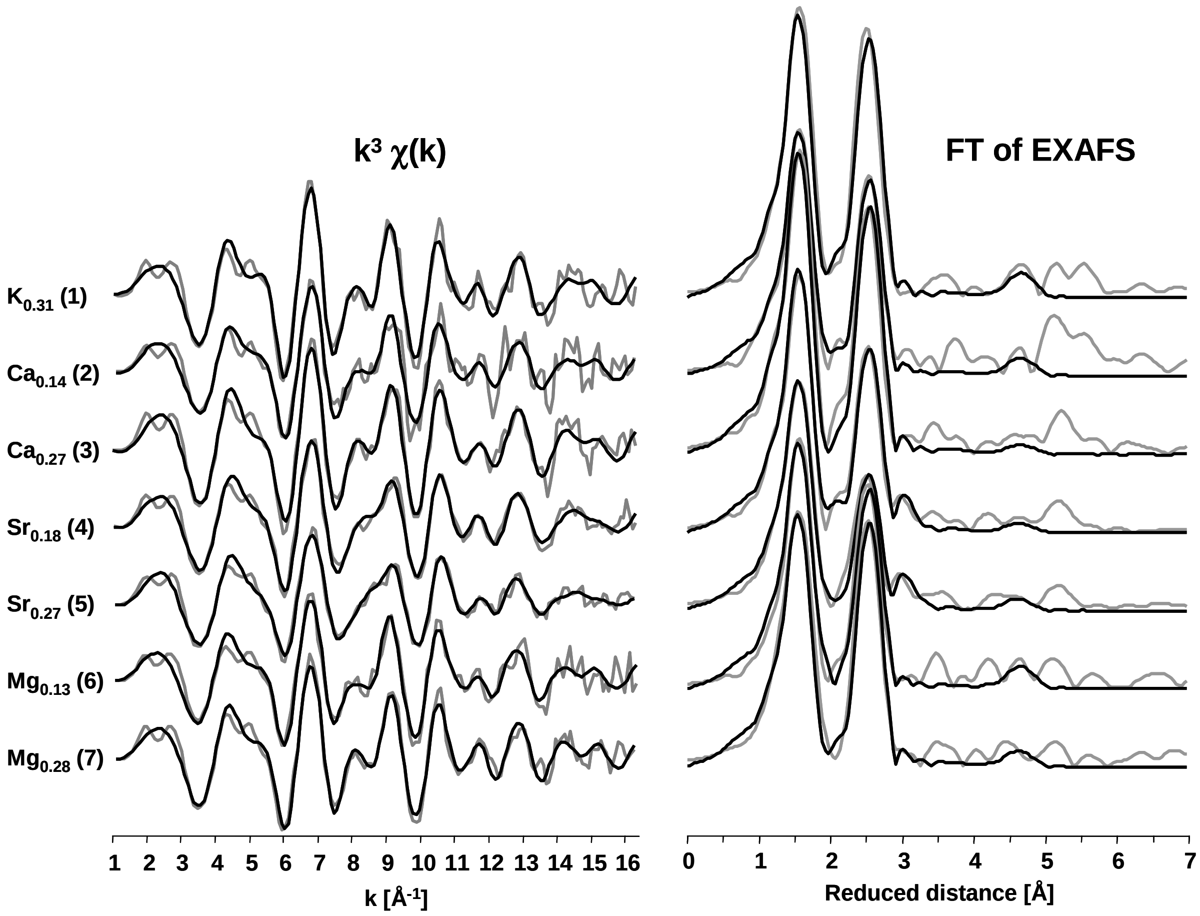

Figure S1. k^3-weighted extended-range EXAFS spectra (left) and their Fourier transforms (FT, right) for oxides 1 – 7. The experimental spectra are shown as gray lines and simulation results for the fit with one short Mn–Mn distance are shown in black. The fit parameters are given in Table S3. The relatively high value obtained for the Debye-Waller parameter for the short Mn–Mn distance indicates that there is probably a second short distance, as shown in the fit presented in Fig. S2.

Table S3. Parameters obtained by simulation of the k^3-weighted EXAFS spectra (*N*, coordination number; *R*, absorber-backscatter distance; σ, Debye-Waller parameter). The errors are given in gray and represent the 68% confidence interval of the respective fit parameter. The sum of the coordination numbers in the first two oxygen shells was fixed to 6. The Debye-Waller parameter, σ, was kept equal for the two oxygen shells (indicated with „=“ in the table) and was fixed for the longer Mn–Mn distance and for the Mn–Sr distance (values marked with asterisks, *).

		$K_{0.31}$ (1)	$Ca_{0.14}$ (2)	$Ca_{0.27}$ (3)	$Sr_{0.18}$ (4)	$Sr_{0.27}$ (5)	$Mg_{0.13}$ (6)	$Mg_{0.28}$ (7)
Mn–O	***R*, Å**	**1.90**/0.01	**1.90**/0.01	**1.91**/0.01	**1.90**/0.01	**1.91**/0.01	**1.90**/0.01	**1.90**/0.01
	N	**4.9**/0.4	**4.5**/0.4	**5.1**/0.4	**4.7**/0.3	**4.7**/0.3	**4.6**/0.3	**4.9**/0.3
	***σ*, Å**	**0.058**/0.006	**0.063**/0.006	**0.058**/0.005	**0.062**/0.005	**0.068**/0.004	**0.061**/0.006	**0.066**/0.006
Mn–O	***R*, Å**	**2.29**/0.04	**2.28**/0.03	**2.27**/0.05	**2.30**/0.03	**2.26**/0.02	**2.24**/0.03	**2.28**/0.04
	N	**1.1**/0.4	**1.5**/0.4	**0.9**/0.4	**1.3**/0.3	**1.3**/0.3	**1.4**/0.3	**1.1**/0.3
	***σ*, Å**	=	=	=	=	=	=	=
Mn–Mn	***R*, Å**	**2.88**/0.01	**2.88**/0.01	**2.88**/0.01	**2.87**/0.01	**2.87**/0.01	**2.88**/0.01	**2.88**/0.01
	N	**5.0**/1.0	**3.2**/0.8	**3.8**/0.8	**2.9**/0.7	**2.2**/0.6	**3.2**/0.8	**3.6**/0.7
	***σ*, Å**	**0.079**/0.008	**0.072**/0.011	**0.069**/0.009	**0.070**/0.009	**0.073**/0.011	**0.071**/0.010	**0.067**/0.008
Mn–Mn	***R*, Å**	**5.02**/0.05	**4.99**/0.07	**4.99**/0.13	**4.97**/0.11	**4.95**/0.07	**5.00**/0.05	**4.97**/0.07
	N	**1.7**/1.6	**1.2**/1.6	**0.6**/1.5	**0.6**/1.2	**0.8**/1.0	**1.5**/1.5	**1.1**/1.4
	***σ*, Å**	**0.067***	**0.067***	**0.067***	**0.067***	**0.067***	**0.067***	**0.067***
Mn–Sr	***R*, Å**				**3.33**/0.03	**3.32**/0.02		
	N				**0.5**/0.3	**0.5**/0.3		
	***σ*, Å**				**0.063***	**0.063***		
	R_F, %	18.0	21.1	16.9	15.1	14.9	21.2	18.8

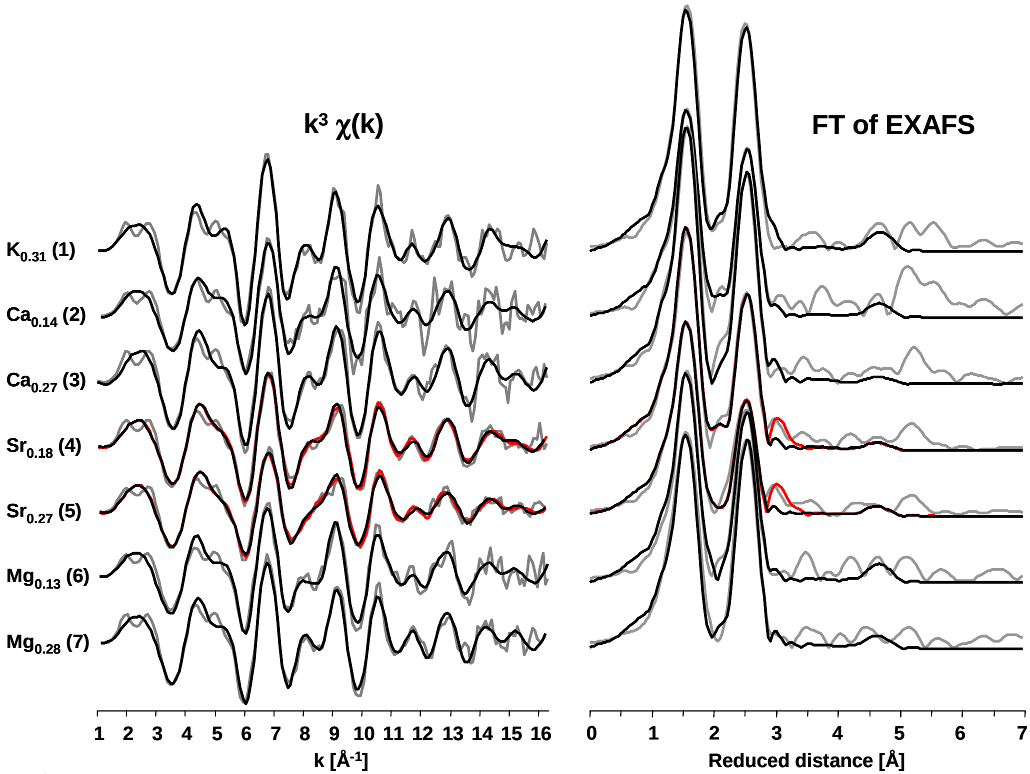

Figure S2. k^3-weighted extended-range EXAFS spectra (left) and Fourier transforms (right) for 1 – 7. The experimental spectra are shown with gray lines and simulation results for the fit with two short Mn–Mn distances are shown in black. The fit parameters are given in Table S4. For Sr-containing samples the black lines show the simulation result without Mn–Sr distance (as done for the rest of the samples) and the red lines represent the fit results if a 3.3 Å Mn–Sr distance is included.

Table S4. Parameters obtained by simulation of the k^3-weighted EXAFS spectra (*N*, coordination number; *R*, absorber-backscatter distance; σ, Debye-Waller parameter). The errors are given in gray and represent the 68% confidence interval of the respective fit parameter. The sum of the coordination numbers in the first two oxygen shells was fixed to 6. The Debye-Waller parameter, σ, was kept equal for the two oxygen shells and for the two short Mn–Mn distances (indicated with „=“ in the table) and was fixed for the longer Mn–Mn distance and for the Mn–Sr distance (values marked with asterisks, *).

		$K_{0.31}$ (1)	$Ca_{0.14}$ (2)	$Ca_{0.27}$ (3)	$Sr_{0.18}$ (4)	$Sr_{0.27}$ (5)	$Mg_{0.13}$ (6)	$Mg_{0.28}$ (7)
Mn–O	***R*, Å**	**1.90**/0.01	**1.90**/0.01	**1.90**/0.01	**1.90**/0.01	**1.90**/0.01	**1.90**/0.01	**1.90**/0.01
	N	**4.9**/0.3	**4.5**/0.4	**5.1**/0.3	**4.7**/0.3	**4.6**/0.3	**4.6**/0.3	**4.9**/0.3
	***σ*, Å**	**0.058**/0.005	**0.062**/0.006	**0.058**/0.005	**0.062**/0.005	**0.067**/0.004	**0.061**/0.006	**0.066**/0.006
Mn–O	***R*, Å**	**2.29**/0.03	**2.28**/0.03	**2.27**/0.04	**2.30**/0.03	**2.26**/0.02	**2.24**/0.03	**2.28**/0.04
	N	**1.1**/0.3	**1.5**/0.4	**0.9**/0.3	**1.3**/0.3	**1.4**/0.3	**1.4**/0.3	**1.1**/0.3
	***σ*, Å**	=	=	=	=	=	=	=
Mn–Mn	***R*, Å**	**2.86**/0.01	**2.87**/0.02	**2.87**/0.01	**2.86**/0.02	**2.86**/0.01	**2.87**/0.02	**2.88**/0.01
	N	**4.0**/0.5	**2.8**/0.7	**3.7**/0.5	**2.5**/0.6	**2.0**/0.4	**2.9**/0.6	**3.5**/0.5
	***σ*, Å**	**0.063***	**0.063***	**0.063***	**0.063***	**0.063***	**0.063***	**0.063***
Mn–Mn	***R*, Å**	**2.99**/0.02	**2.98**/0.07	**3.01**/0.04	**2.97**/0.09	**2.99**/0.06	**2.99**/0.06	**3.00**/0.08
	N	**1.8**/0.5	**0.8**/0.7	**1.0**/0.5	**0.6**/0.6	**0.5**/0.4	**0.9**/0.6	**0.6**/0.5
	***σ*, Å**	=	=	=	=	=	=	=
Mn–Mn	***R*, Å**	**5.03**/0.05	**4.99**/0.07	**5.00**/0.13	**4.97**/0.12	**4.95**/0.07	**5.00**/0.05	**4.97**/0.07
	N	**1.6**/1.4	**1.1**/1.6	**0.6**/1.5	**0.6**/1.3	**0.8**/1.0	**1.5**/1.5	**1.0**/1.4
	***σ*, Å**	**0.067***	**0.067***	**0.067***	**0.067***	**0.067***	**0.067***	**0.067***
Mn–Sr	***R*, Å**				**3.33**/0.03	**3.32**/0.02		
	N				**0.5**/0.3	**0.5**/0.3		
	***σ*, Å**				**0.063***	**0.063***		
	R_F, %	13.8	21.6	16.4	14.7	13.6	20.5	17.9

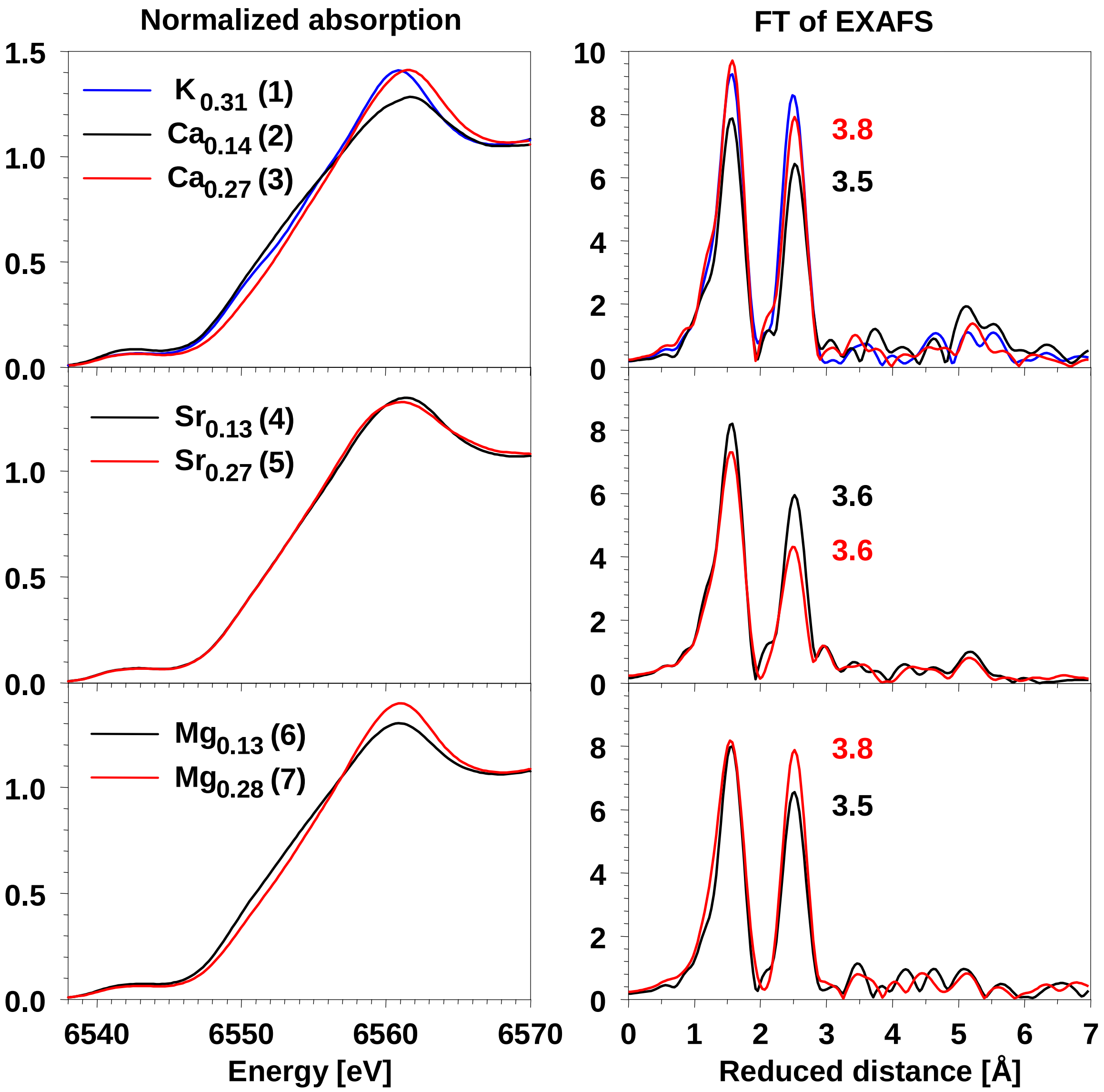

Figure S3. XANES spectra (left) and Fourier transformed EXAFS (right) for the oxides **1-7**. The mean oxidation state of Mn was calculated from the edge positions in XANES spectra after calibration employing Mn oxides of known oxidation state as a reference, see ref.[10]. The Mn oxidation state is indicated with the corresponding color in the right panels. The peak height of the second peak in the Fourier transformed EXAFS spectra appears to correlate with the mean oxidation state of Mn (increased for more oxidized oxide, see the main text).

Oxygen detection by gas chromatography

For oxygen evolution experiments, gas chromatograms were recorded using a HP 6890 Series GC System equipped with a 8 ft x 1/8 in 5 Å molecular sieve column (Supelco) using helium (4.6 quality) as a carrier gas. The gases O_2 and N_2 were monitored by a thermal conductivity detector.

About 5 mg of oxide **1** - **7** (see Table S2) and 685 mg (1.25 mmol) ammonium-cerium^{IV}-nitrate were weighed into 20 mL septum vials. After the addition of 5 mL H_2O, the vials were capped immediately using gas tight septa and the solution was sonicated for 10 s. The headspace gas was injected using a HP 7694 headspace sampler equipped with a 1 mL sample-loop. Six headspace extractions from a single septum vial were taken in intervals of 10 min. Therefore, the multiple headspace extraction value was set to 6, the vial equilibration time of the headspace sampler was set to 8.6 min, pressurize time to 0.10 min, loop fill time to 0.20 min, loop equilibration time to 0.10 min and the injection time to 1.0 min, giving an overall cycle time of 10 min and an overall time of 1 h for each catalytic experiment. The following temperature settings were used: oven temperature

(headspace sampler): 40°C, sample loop temperature: 50°C, transfer line temperature: 65°C, oven temperature (gas chromatograph): 70°C.
The amount of oxygen evolved was calculated from the N_2 signals of air at each measurement. The amount of oxygen from air corresponding to the detected nitrogen peak was calculated and subtracted for every measurement. Because of the pressurization of the septum vials before every measurement, the headspace gas to be analysed is diluted with carrier gas. In addition, leakages can occur after the first insertion of the headspace sampler needle in multiple headspace extraction mode. Thus, the detected values for O_2 and N_2 were corrected by a factor calculated from repeating the experiments as described above, but with only one headspace extraction at the end of the interval of 1 h. All measurements described here were carried out at least three times for each oxide.

For comparison of the detected oxygen evolution values, the oxygen evolution rates have to be scaled. As manganese is the only capable element for redox processes occurring during water oxidation catalysis present in birnessites **1**-**7**, oxygen evolution rates can be scaled to the amount of manganese (See Figure S11). Other possible methods to calculate oxygen evolution rates are to scale the amount of evolved oxygen per catalyst mass or surface area (See Figure S12, S13). But as both parameters vary independently for birnessites **1**-**7**, the results are hardly comparable. Thus, we decided to present oxygen evolution rates scaled to the amount of manganese and calculated them as mmol O_2 per mol Mn.

Additional figures

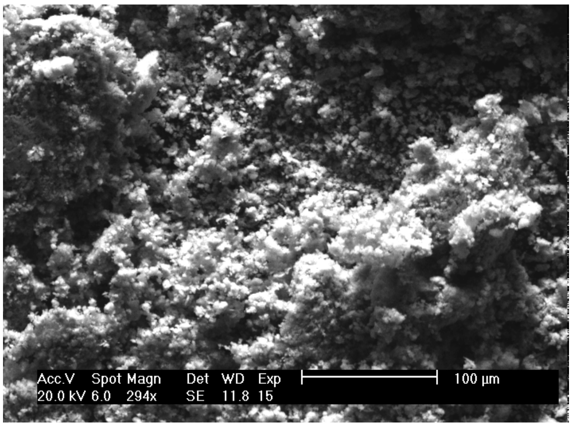

Figure S4. SEM image of $K_{0.31}$-birnessite (**1**).

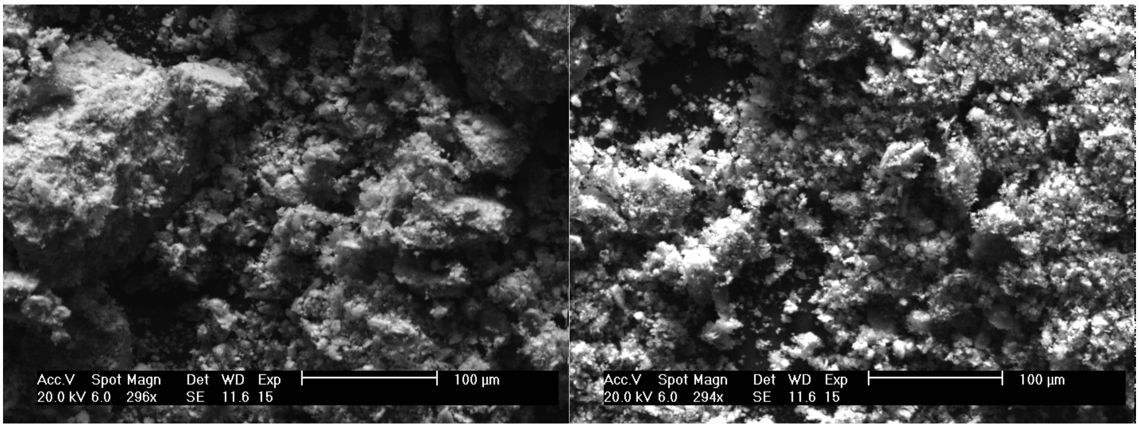

Figure S5. SEM image of *left:* $Ca_{0.14}$-birnessite (**2**), *right:* $Ca_{0.27}$-birnessite (**3**).

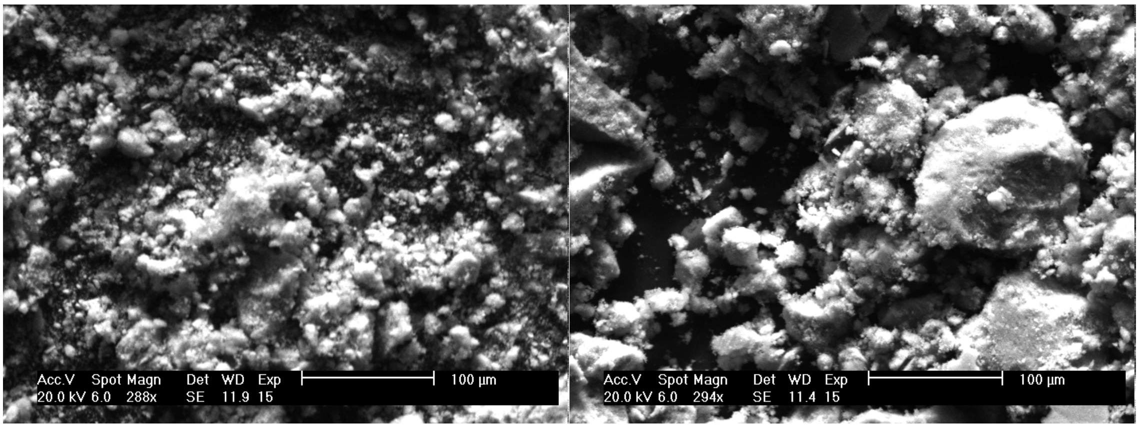

Figure S6. SEM image of *left:* $Sr_{0.18}$-birnessite (**4**), *right:* $Sr_{0.27}$-birnessite (**5**).

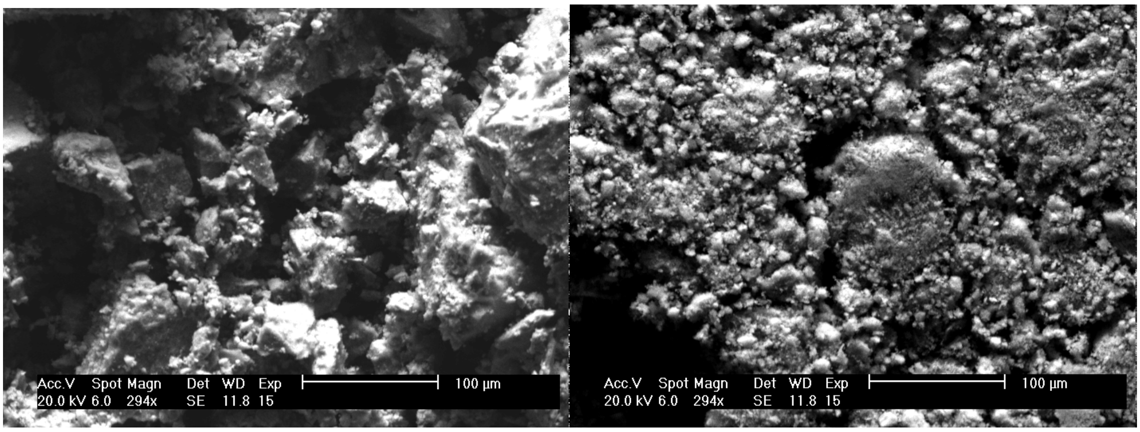

Figure S7. SEM image of *left:* $Mg_{0.13}$-birnessite (**6**), *right:* $Mg_{0.28}$-birnessite (**7**).

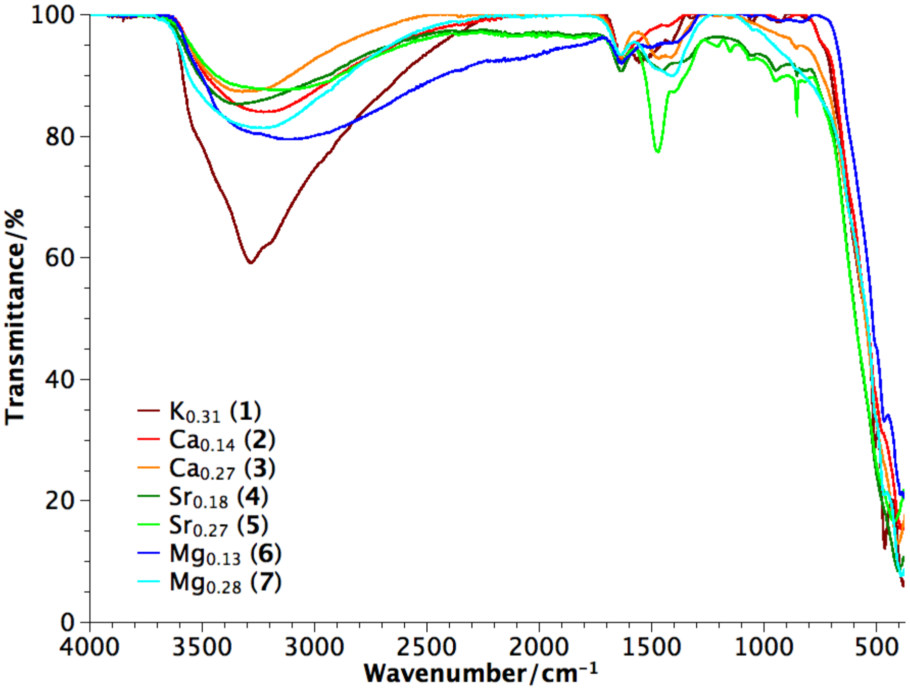

Figure S8. ATR-IR-spectra of birnessites **1-7**.

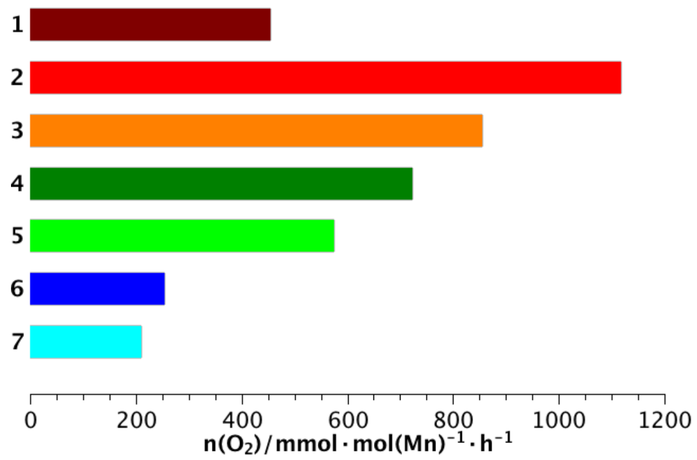

Figure S9. Oxygen evolution rates of M-birnessites **1-7** shown as the amount of evolved oxygen per manganese.

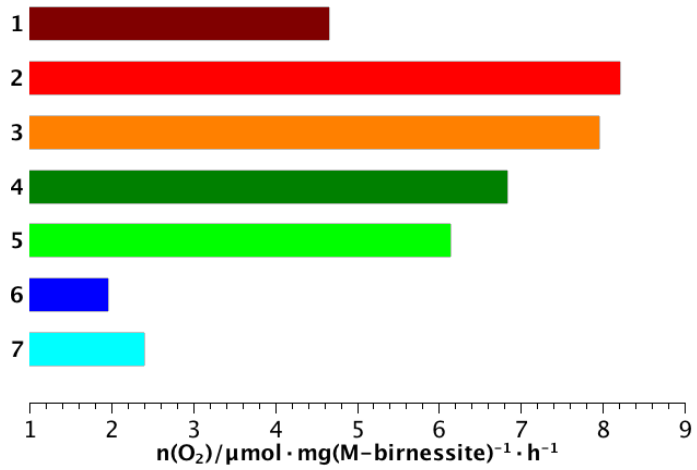

Figure S10. Oxygen evolution rates of M-birnessites **1-7** shown as the amount of evolved oxygen per oxide mass.

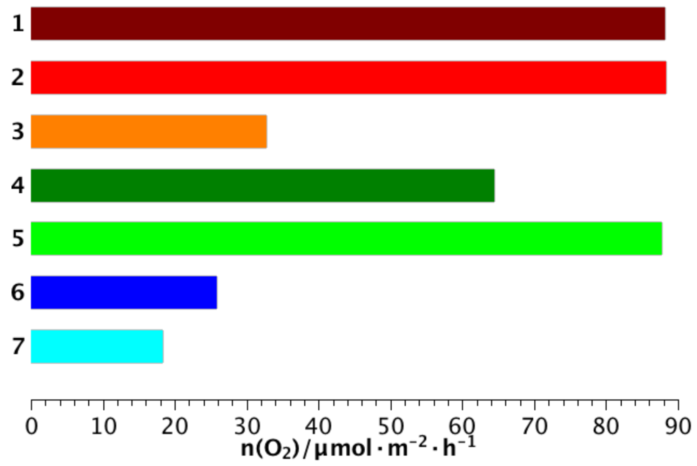

Figure S11. Oxygen evolution rates of M-birnessites **1-7** shown as the amount of evolved oxygen per surface area.

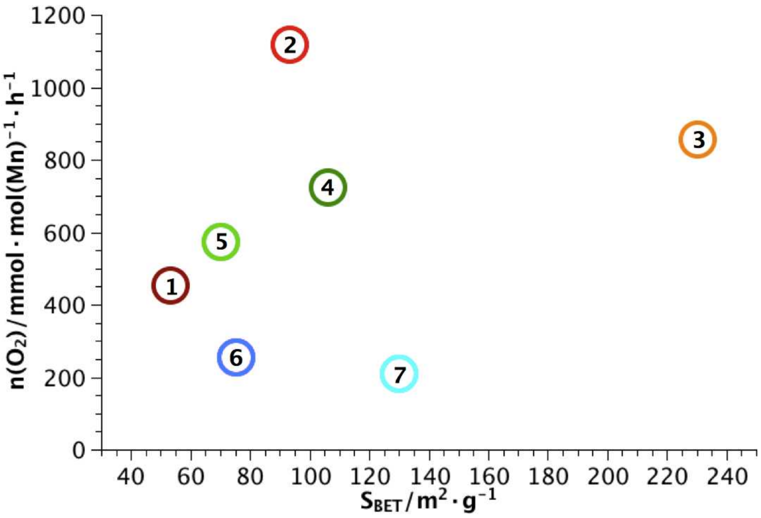

Figure S12. Comparison of the catalytic activity for water oxidation of birnessites **1-7** *vs.* surface area.

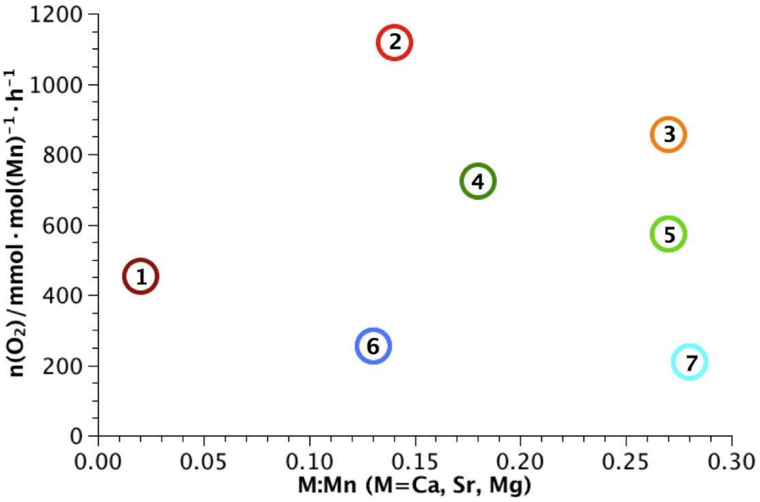

Figure S13. Comparison of the catalytic activity for water oxidation of birnessites **1-7** *vs.* the ratio of the amount of alkaline earth cations to manganese cations.

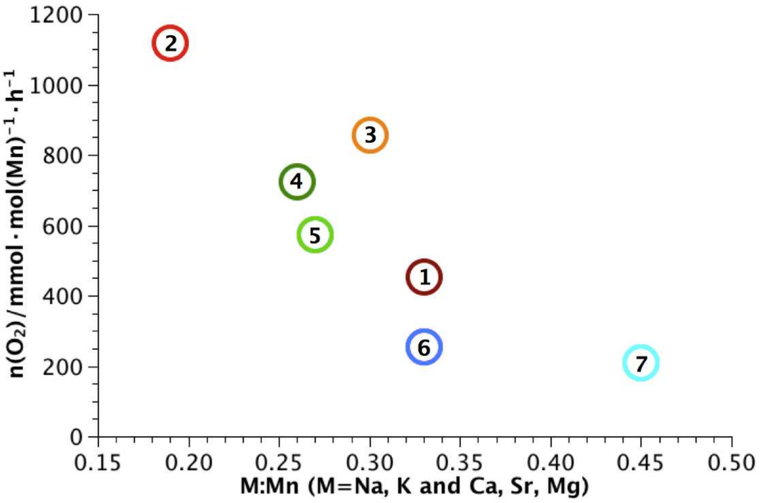

Figure S14. Comparison of the catalytic activity for water oxidation of birnessites **1-7** *vs.* the ratio of non manganese cations to manganese ions.

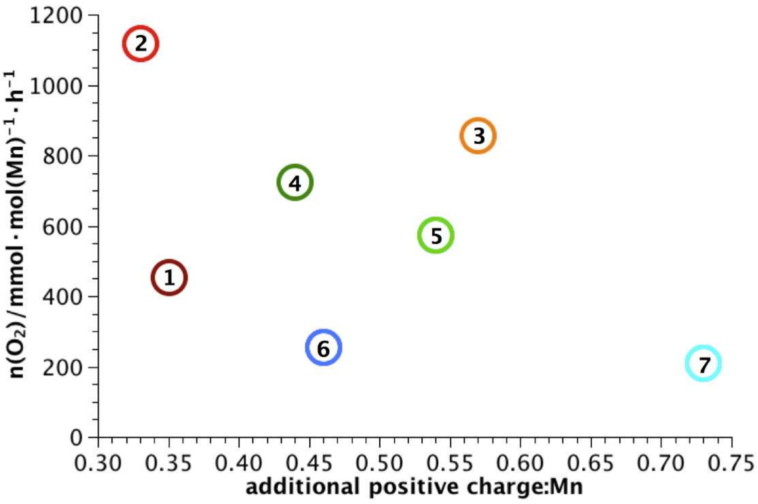

Figure S15. Comparison of the catalytic activity for water oxidation of birnessites **1-7** *vs.* the amount of positive charge additional to manganese cations.

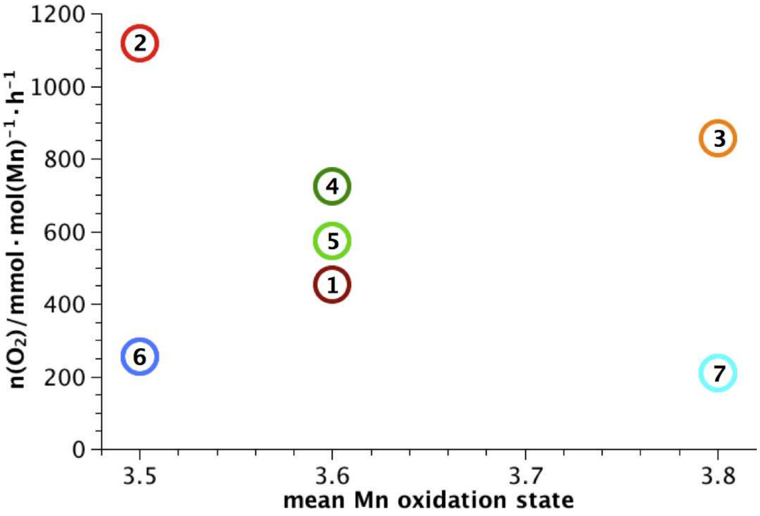

Figure S16. Comparison of the catalytic activity for water oxidation of birnessites **1-7** *vs.* the mean oxidation state of manganese.

References

1 J. Luo, Q. Zhang, A. Huang, O. Giraldo and S. L. Suib, *Inorg. Chem.*, 1999, **38**, 6106.
2 H. Dau, P. Liebisch and M. Haumann, *Anal. Bioanal. Chem.*, 2003, **376**, 562.
3 J. E. Penner-Hahn, *Coord. Chem. Rev.*, 1999, **190-192**, 1101.
4 J. J. Rehr and R. C. Albers, *Rev. Mod. Phys.*, 2000, **72**, 621.
5 A. L. Ankudinov, B. Ravel, J. J. Rehr and S. D. Conradson, *Phys. Rev. B Condens. Matter Mater. Phys.*, 1998, **58**, 7565.
6 W. H. Press, S. A. Teukolsky, W. T. Vetterling and B. P. Flannery, *Numerical Recipes in C: The Art of Scientific Computing*, *Second Edition*, Cambridge University Press, Cambridge-New York-Port Chester-Melbourne-Sydney, 1992.
7 E. A. Stern, *Phys. Rev. B*, 1993, **48**, 9825.
8 W. T. Eadie, D. Drijard, F. E. James, M. Roos and B. Sadoulet, *Statistical methods in experimental physics*, *Second Edition*, North Holland, Amsterdam, 1971.
9 C. Meinke, V. A. Sole, P. Pospisil and H. Dau, *Biochemistry*, 2000, **39**, 7033.
10 I. Zaharieva, M. M. Najafpour, M. Wiechen, M. Haumann, P. Kurz and H. Dau, *Energy Environ. Sci.*, 2011, **4**, 2400.